

XUV-laser spectroscopy on the $c'_4 \ ^1\Sigma_u^+$, $v=0$ and $c_3 \ ^1\Pi_u$, $v=0$ Rydberg states of N_2

Pieter F. Levelt and Wim Ubachs

Laser Centre Free University, Department of Physics and Astronomy, De Boelelaan 1081, 1081 HV Amsterdam, The Netherlands

Received 4 November 1991

The $c'_4 \ ^1\Sigma_u^+$, $v=0$ and $c_3 \ ^1\Pi_u$, $v=0$ Rydberg states of N_2 are studied by means of 1 XUV + 1 UV resonance enhanced two-photon ionization. The experimental resolution (0.35 cm^{-1} fwhm) combined with a calibration against a visible wavelength I_2 standard results in an order of magnitude better accuracy in the absolute line positions than in previous non-laser based investigations. The effects of homogeneous and heterogeneous perturbations of the Rydberg states by $b \ ^1\Sigma_u^+$ and $b \ ^1\Pi_u$ valence states are analyzed.

1. Introduction

Unactivated molecular nitrogen is transparent for radiation at wavelengths longer than 100 nm, apart from some weak absorption bands, such as the $a \ ^1\Pi_g - X \ ^1\Sigma_g^+$ system around 150 nm [1]. However, just below 100 nm in the extreme ultraviolet (XUV) a congested and complex electric dipole allowed absorption spectrum starts extending to a wavelength of 79.5 nm. This corresponds to the energy of the first ionization limit. Initially the complex features, observed in absorption [2] and partly in emission [3,4], were interpreted as composed of a multitude of band systems. Through the important and extensive investigations of Lefebvre-Brion [5], Dressler [6] and Carroll, Collins and Yoshino [7,8] it is established now that the complex XUV absorption spectrum of N_2 can be explained in terms of two valence states, denoted $b \ ^1\Sigma_u^+$ and $b \ ^1\Pi_u$, and two Rydberg series $c'_n \ ^1\Sigma_u^+$ and $c_n \ ^1\Pi_u$ converging to the first ionization limit ($X \ ^2\Sigma_g^+$) of N_2^+ . Additionally Rydberg series such as $o_n \ ^1\Pi_u$ [9], converging to the second ionization limit ($A \ ^2\Pi_u$) play a role.

The analysis of the energy level structure above 100000 cm^{-1} in N_2 has been a tremendous task because of the many homogeneous and heterogeneous perturbations. Two different strategies were followed to unravel the manifolds of mutually interacting vibronic states. Stahel et al. [10] succeeded to explain

the irregular energy spacings as well as the anomalous intensity behaviour in the vibrational ladders based on a model of non-adiabatic representations of all $^1\Sigma_u^+$ and $^1\Pi_u$ states. States of different electronic symmetry were treated separately. Alternatively, interactions between Rydberg series $c'_n \ ^1\Sigma_u^+$ and $c_n \ ^1\Pi_u$ were treated within the framework of l -uncoupling [8]. In limited energy regions homogeneous and heterogeneous couplings could be incorporated simultaneously as was shown by Yoshino and Freeman [11] for the Rydberg states $c'_5 \ ^1\Sigma_u^+$, $v=0$ and $c_4 \ ^1\Pi_u$, $v=0$, interacting with various valence states of Σ and Π symmetry. The local perturbation between the $c'_4 \ ^1\Sigma_u^+$, $v=0$ Rydberg state and the $b' \ ^1\Sigma_u^+$, $v=1$ valence state was analyzed by Yoshino and Tanaka [12].

The spectroscopic data used in these perturbation analyses were collected using classical radiation sources. In recent years the advance of high power lasers and non-linear wave-mixing techniques have opened the possibility for high resolution XUV-laser spectroscopic studies. Trickl et al. [13] populated the $c'_4 \ ^1\Sigma_u^+$ state of N_2 with an XUV laser for subsequent laser-excitation of high-lying Rydberg states of N_2 . Ubachs et al. [14] investigated in high resolution the $b \ ^1\Pi_u$, $v=0$ and 1 states of $^{14}N_2$ and $^{14}N^{15}N$ also using an XUV-laser source. In the present work we use a similar XUV-laser setup for a spectroscopic study of the lowest Rydberg states of Π and Σ character in N_2

and their local perturbations by nearby valence states. The interest in these states originates from the fact that in the upper regions of planetary atmospheres N_2 , excited by electron collisions, produces XUV emissions predominantly through the $c'_4 \ ^1\Sigma_u^+$ state [15,16]. The spectroscopic data for the $c'_4 \ ^1\Sigma_u^+$, $v=0$ state and the interacting $b' \ ^1\Sigma_u^+$, $v=1$ state are recorded with an absolute accuracy of 0.04 cm^{-1} , which is almost an order of magnitude more accurate than in previous classical studies. The slightly weaker transition to the $c_3 \ ^1\Pi_u$, $v=0$ state was also investigated. Prior to the present work no line positions for this lowest Rydberg state of N_2 were reported although a preliminary analysis was performed by Carroll and Collins [7] in their study of the $b \ ^1\Pi_u$ valence state.

2. Experimental

A detailed description of the XUV-laser setup will be presented elsewhere [17], therefore only a short overview will be given here. The XUV spectrometer consists of a laser setup with an injection seeded Nd:YAG laser (QuantaRay GCR4) pumping a dye laser (QuantaRay PDL3), and of a vacuum setup with three differentially pumped high-vacuum chambers. In the first chamber the third harmonic of the UV-laser light from the frequency-doubled dye laser is generated in a free flowing jet of xenon gas underneath the orifice of a pulsed nozzle. The resulting extreme ultraviolet (XUV) radiation and the overlapping UV travel through a pinhole into the second vacuum chamber. Here the light beams perpendicularly intersect a molecular beam. This beam is obtained through a skimmer from a pulsed valve positioned in the third chamber. Variation of the timing characteristics of the pulsed valve enabled the production of a probe gas molecular beam with either a cold (40 K) or an almost room temperature rotational distribution in the molecular beam.

The spectra were recorded by the technique of 1 XUV + 1 UV resonance enhanced two-photon ionization. The $N_2 \ X \ ^1\Sigma_g^+$ ground state molecules are excited into the states under investigation after resonant absorption of an XUV photon, and subsequently ionized by nonresonant absorption of a UV photon. In the interaction region an electric field of about 100

V/cm is applied to extract ions produced into a 20 cm time-of-flight (TOF) tube. At the end of this tube the particles are detected on an electron multiplier connected to a boxcar integrator. The mass-selectivity of the TOF setup ensures that the N_2^+ -ion signal can be separated from the background ions.

The XUV power was not calibrated but based on published data [18] we roughly estimate a density of 10^9 photons/pulse at input power levels of about 15 mJ in the UV. It should be noted that because of focusing conditions ($f=20$ cm) underneath the frequency-tripling nozzle the light beams diverge into the interaction zone and span an area of 1.5 cm diameter. The spectral characteristics of the XUV spectrometer are determined mainly by the properties of the Nd:YAG dye-laser combination. The bandwidth of the dye laser is about 0.07 cm^{-1} , the pulse duration 5 ns. The minimum linewidth (fwhm) observed in the XUV spectra is 0.35 cm^{-1} . Under the assumption of a perfectly Gaussian temporal profile of the laser pulse a bandwidth in the XUV of $\Delta\omega_{\text{XUV}} = \sqrt{6} \Delta\omega_{\text{dye}}$, so of 0.17 cm^{-1} might be expected. In the crossed-beam setup Doppler contributions to the spectral linewidth may be ignored. The additional broadening must be due to a non-perfect temporal beam profile.

Simultaneously with the XUV excitation spectra of N_2 absorption spectra of I_2 were recorded. To generate this absorption spectrum in the visible wavelength range a small fraction of the fundamental of the dye laser was used. The line positions of the N_2 resonances were obtained through interpolation between selected unblended and symmetric I_2 lines. This procedure was performed by computer. The absolute accuracy in the I_2 standard is 0.002 cm^{-1} in the visible [19,20] and thus 0.012 cm^{-1} for the XUV line positions. The correction to the absolute energy positions of I_2 lines [20] was accounted for in the calibration. Due to the linewidth of N_2 and I_2 resonances the transition frequencies of the unblended N_2 spectral lines with good signal-to-noise could be determined to within 0.04 cm^{-1} by fitting Gaussian profiles to the observed features. For blended lines a deconvolution procedure was followed resulting in somewhat larger uncertainties.

In the recording of the spectra care was taken to avoid effects of high laser power that may result in line broadening above the minimum of 0.35 cm^{-1} .

At UV-input powers exceeding 20 mJ/pulse asymmetric broadening effects were observed, particularly on the c'_4-X transitions. By varying tripling gas density, and therewith the harmonic conversion efficiency, as well as the UV-input intensity we found that the broadening is due to saturation of the resonant one photon XUV transition as well as to UV-power induced ac Stark and population depletion effects. A quantitative analysis of these processes is under way, but for the present spectroscopic study to determine positions of unbroadened lines the outcome will have no consequences.

3. Results and analysis

3.1. The $c'_4 \ ^1\Sigma_u^+$, $v=0$ Rydberg state

Fig. 1 shows the XUV excitation spectrum of N_2 in the wavelength range $\lambda=95.75-96.0$ nm. All lines were identified to belong to the $c'_4 \ ^1\Sigma_u^+ - X \ ^1\Sigma_g^+$ (0,

0) and $b' \ ^1\Sigma_u^+ - X \ ^1\Sigma_g^+$ (1, 0) bands with a few exceptions that could be assigned to high J transitions of the $b \ ^1\Pi_u - X \ ^1\Sigma_g^+$ (5, 0) band. The latter features are marked with a cross in fig. 1. Near P(11) and P(12) a local perturbation clearly manifests itself in the irregular spacing of lines in the c'_4-X band. In the R branch there is a similar effect at R(9) and R(10). The improvement in resolution shows at first glance in a comparison of the XUV laserspectrum of fig. 1 with the densitometer trace of the previous highest resolution classical absorption spectrum (see fig. 1 of ref. [12]). Some I_2 resonances used for the calibration of XUV excitation lines are marked with the number of the I_2 atlas [19].

The spectrum of fig. 1 was recorded by excitation of a pulsed effusive beam with a near room-temperature population distribution over rotational states. Under these conditions the $b'-X$ (1, 0) bandhead is overlapped by high J lines such as the P(20) of the $b \ ^1\Pi_u - X$ (5, 0) band. In fig. 2 a spectrum of the $b'-X$ bandhead is shown, this time recorded under the

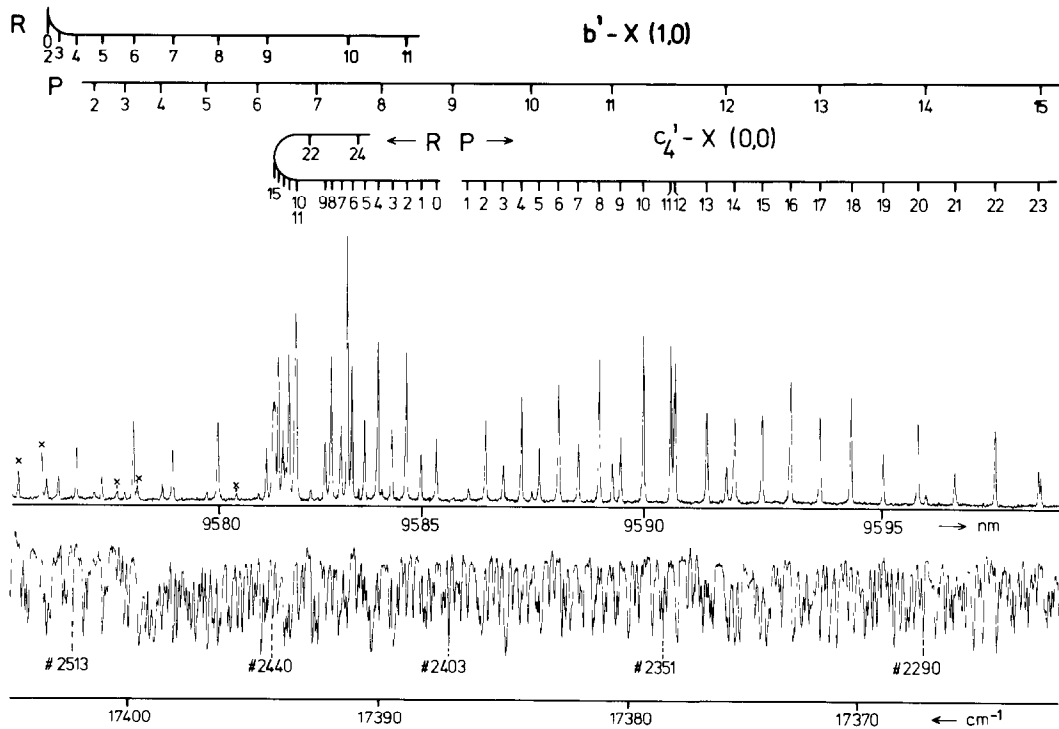


Fig. 1. Upper part: 1 XUV + 1 UV resonance-enhanced two-photon ionization spectrum of the $b' \ ^1\Sigma_u^+ - X \ ^1\Sigma_g^+$ (1, 0) and $c'_4 \ ^1\Sigma_u^+ - X \ ^1\Sigma_g^+$ (0, 0) transitions in N_2 . Lines marked with a cross are excitations to high J states of the $b \ ^1\Pi_u - X \ ^1\Sigma_g^+$ (5, 0) band. Lower part: I_2 -absorption spectrum recorded in the visible. Lines marked with (#) refer to the number in the I_2 atlas ref. [19].

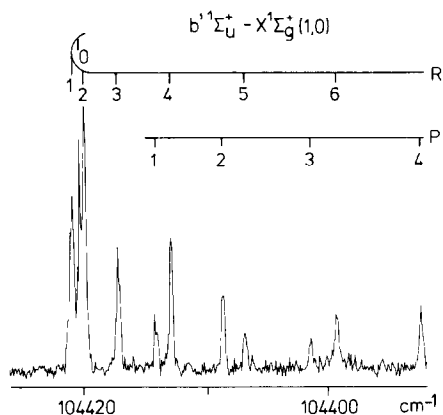


Fig. 2. Bandhead part of the $b' \ ^1\Sigma_u^+ - X \ ^1\Sigma_g^+ (1, 0)$ transition in N_2 as obtained from a cold molecular beam.

conditions of a pulsed supersonically cooled expansion of pure N_2 . Here the distribution peaks at $J=2$ and all disturbing $b-X (5, 0)$ features have disappeared, so that an unambiguous assignment of the low J states can be performed. In the present analysis spectroscopic data of various recordings of “warm” and “cold” spectra were incorporated. In tables 1 and 2 the experimentally determined line positions for the $c'_4-X (0, 0)$ and $b'-X (1, 0)$ are given with their estimated errors.

The experimental data of all observed P and R lines of both c'_4-X and $b'-X$ bands were fitted to the simple formula for the rotational energy of a diatomic molecule in a Σ state (ground state as well as excited states):

$$E_{\Sigma} = BJ(J+1) - DJ^2(J+1)^2. \quad (1)$$

Here B is the rotational constant and D the centrifugal distortion coefficient. For the $X \ ^1\Sigma_g^+, v=0$ ground state of N_2 the most accurately known values of the spectroscopic constants were used. Dunham coefficients Y_{ij} , obtained from low pressure electric quadrupole absorption measurements by Rinsland et al. [21], were used to calculate B_0 and D_0 :

$$B_0 = -Y_{01} - \frac{1}{2}Y_{11} = 1.989582(4) \text{ cm}^{-1},$$

$$D_0 = -Y_{02} = 5.761(10) \times 10^{-6} \text{ cm}^{-1}.$$

These constants were fixed at the above values throughout the present analysis.

The perturbation between the $c'_4(0)$ and the $b'(1)$ states was analyzed following the treatment of Yosh-

ino and Freeman [11]. It requires diagonalization of a matrix of the form

$$\begin{pmatrix} E_{b'\Sigma} & H_{c'_4b'} \\ H_{c'_4b'} & E_{c'_4\Sigma} \end{pmatrix},$$

where $H_{c'_4b'}$ represents the matrix element for a homogeneous interaction between the excited $^1\Sigma_u^+$ states.

The spectroscopic data of tables 1 and 2 were included in a least squares minimization routine, in which the band origins, the rotational constants of the excited states and the interaction parameter $H_{c'_4b'}$ were varied. Conversion of the fit was poor when the highest J states were included. Therefore the fitting procedure was limited to data up to $J=19$ for the excited states. The constants obtained and the uncertainties derived from the covariance matrix are listed in table 3. Moreover deviations between observed and calculated values for the line positions are included in tables 1 and 2. The quality of the fit is demonstrated by the resulting normalized χ^2 , which has a value of 1.0 when using the estimated errors of tables 1 and 2. The energy values for the states with $J \geq 20$ have a strong tendency to shift downward with respect to the extrapolated values from the constants derived for low J states. Quantitatively this tendency is similar in P and R branch, thus confirming the correct assignment of these lines.

The homogeneous local perturbation in between $J=10$ and 11 results in a typical anticrossing pattern when the term values of $c'_4(0)$ and the $b'(1)$ rotational states are plotted against $J(J+1)$ as is shown in fig. 3. A value of the interaction matrix element $H_{c'_4b'} = 5.072 \text{ cm}^{-1}$ results in a maximum shift of 2.6 cm^{-1} at $J=11$. The symmetrical pattern in fig. 3 indicates that the local perturbation is of homogeneous nature (see also ref. [22]). For some yet unexplained reason the intensity in the R branch of $b'-X$ is too weak to observe lines beyond R(10), although R(10) itself is strong.

The combination of high-resolution wavelength selection with a TOF mass spectrometer allows for a spectroscopic investigation of $^{14}N^{15}N$ molecules. Fig. 4 shows a recording of an XUV excitation spectrum of the $c'_4-X (0, 0)$ band in natural N_2 (with 0.74% $^{14}N^{15}N$) measured with the gated integrator set at mass 29. In this spectrum still some signal of $^{14}N_2$ is visible. This is caused by $^{14}N_2^+$ ions arriving at late

Table 1

Observed line positions (in cm^{-1}) for R(J) and P(J) lines of the $c'_4 \ ^1\Sigma_u^+ - X \ ^1\Sigma_g^+$ (0, 0) band and deviations from a fit. The position of strong and unblended lines was determined to within 0.04 cm^{-1} . In other cases the error was estimated to be 0.08 cm^{-1}

R(J)			P(J)	
J	observed	obs. – calc.	observed	obs. – calc.
0	104326.51 ± 0.04	0.00		
1	104330.13 ± 0.04	–0.11	104318.62 ± 0.04	–0.05
2	104333.77 ± 0.08	–0.08	104314.65 ± 0.04	0.08
3	104337.32 ± 0.04	0.01	104310.31 ± 0.04	–0.03
4	104340.60 ± 0.04	–0.04	104305.98 ± 0.04	–0.01
5	104343.82 ± 0.04	0.01	104301.57 ± 0.04	0.06
6	104346.85 ± 0.04	0.07	104296.87 ± 0.04	–0.01
7	104349.54 ± 0.04	0.02	104292.06 ± 0.04	–0.03
8	104351.84 ± 0.04	–0.05	104287.08 ± 0.04	–0.03
9	104353.22 ± 0.04	–0.02	104281.93 ± 0.04	0.03
10	104360.31 ± 0.04	0.04	104276.37 ± 0.04	0.04
11	104360.71 ± 0.04	0.04	104269.75 ± 0.04	0.02
12	104362.04 ± 0.08	–0.01	104268.76 ± 0.04	–0.06
13	104363.42 ± 0.08	0.03	104261.26 ± 0.04	–0.02
14	104364.52 ± 0.04	0.03	104254.68 ± 0.04	–0.05
15	104365.28 ± 0.08	–0.01	104248.09 ± 0.04	–0.04
16	104365.73 ± 0.08	–0.01	104241.29 ± 0.08	–0.01
17			104234.22 ± 0.08	0.04
18			104226.77 ± 0.04	0.05
19			104218.84 ± 0.04	–0.02
20	104362.75 ± 0.08 ^{a)}	–0.55	104210.59 ± 0.04	–0.01
21			104201.63 ± 0.04 ^{a)}	–0.25
22	104356.72 ± 0.08 ^{a)}	–2.26	104191.98 ± 0.08 ^{a)}	–0.67
23			104181.63 ± 0.08 ^{a)}	–1.27
24	104345.31 ± 0.08 ^{a)}	–6.85	104170.65 ± 0.08 ^{a)}	–1.94
25			104157.77 ± 0.08 ^{a)}	–3.88

^{a)} Not used in the minimization routine.

times, and thus leaking into the mass-29 channel. These ions are produced in an off-axis region, geometrically further away from the TOF tube and ion detector. This effect causes the line profile of $^{14}\text{N}_2$ resonances to be asymmetric and broadened. For the $^{14}\text{N}^{15}\text{N}$ resonances this is not the case and the line-width reflects the resolution of 0.35 cm^{-1} . In table 4 the observed line positions of $^{14}\text{N}^{15}\text{N}$ resonances are listed. Spectroscopic parameters of the $c'_4(0)$ state of $^{14}\text{N}^{15}\text{N}$ were derived as well (and listed in table 4) in a routine where the ground state constants were fixed at the values of Bendtsen [23].

As only states up to $J=3$ were observed no improvement in the molecular constants derived by Yoshino and Tanaka [12] from observation of states

up to $J=22$, albeit at somewhat lower resolution, was obtained.

3.2. The $c_3 \ ^1\Pi_u, v=0$ Rydberg state

The lowest Rydberg state, assigned $c_3 \ ^1\Pi_u, v=0$, was investigated as well. Fig. 5 displays a spectrum of the bandhead region of the c_3-X transition recorded under conditions of a hot J distribution. In this spectrum the highest J transitions of the c'_4-X and $b'-X$ bands, P(25) and P(16) respectively, also show. Moreover a weak but reproducible line appears, which is the only unidentified line in the present study. Spectral line positions, observed in several scans of hot and cold J distributions, were determined using the I_2 -calibration procedure and are listed in table 5.

Table 2

Observed line positions (in cm^{-1}) for R(J) and P(J) lines of the $b' \ ^1\Sigma_u^+ - X \ ^1\Sigma_g^+ (1, 0)$ band and deviations from a least-squares fit (constants of table 3). The position of strong and unblended lines was determined to within 0.04 cm^{-1} . In other cases the error was estimated to be 0.08 cm^{-1}

R(J)			P(J)	
J	observed	obs. - calc.	observed	obs. - calc.
0	104420.39 ± 0.04	-0.09		
1	104421.06 ± 0.04	-0.04	104414.16 ± 0.04	-0.04
2	104420.07 ± 0.04	0.02	104408.66 ± 0.04	0.12
3	104417.26 ± 0.04	-0.06	104401.21 ± 0.04	0.00
4	104412.97 ± 0.04	0.05	104392.19 ± 0.04	-0.00
5	104406.85 ± 0.04	-0.01	104381.57 ± 0.04	0.06
6	104399.20 ± 0.04	0.06	104369.15 ± 0.04	-0.01
7	104389.75 ± 0.04	-0.05	104355.04 ± 0.08	-0.10
8	104378.98 ± 0.04	0.02	104339.54 ± 0.08	0.07
9	104367.23 ± 0.04	-0.03	104322.34 ± 0.08	0.16
10	104347.96 ± 0.04	-0.02	104303.35 ± 0.04	-0.05
11			104283.79 ± 0.04	0.04
12			104256.52 ± 0.04	-0.01
13				
14			104208.66 ± 0.08	0.10
15			104181.17 ± 0.08	-0.02
16			104151.86 ± 0.08	-0.21

Table 3

Spectroscopic parameters for the excited states under investigation (all in cm^{-1}). Only data up to $J \leq 20$ were included in the minimization routines

$c_4' \ ^1\Sigma_u^+, v=0$ Rydberg state
$B = 1.9314 \pm 0.0002$
$D = 8.15 \pm 0.07 \times 10^{-5}$
$\nu_0 = 104322.91 \pm 0.02$
$H_{c_4, b'} = 5.027 \pm 0.017$
$b' \ ^1\Sigma_u^+, v=1$ valence state
$B = 1.1486 \pm 0.0002$
$D = 0.86 \pm 0.14 \times 10^{-5}$
$\nu_0 = 104417.91 \pm 0.01$
$H_{c_4, b'} = 5.027 \pm 0.017$
$c_3 \ ^1\Pi_u, v=0$ Rydberg state
$B = 1.5087 \pm 0.0004$
$D = 4.53 \pm 0.05 \times 10^{-5}$
$\nu_0 = 104138.48 \pm 0.04$
$q_x = 0.0234 \pm 0.003$
$q_x^P = 2.86 \pm 0.04 \times 10^{-3}$

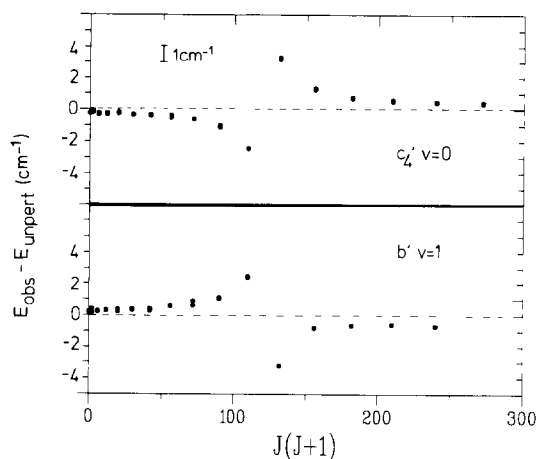


Fig. 3. Plot of the effect of the local perturbation between $c_4' \ ^1\Sigma_u^+, v=0$ (upper part) and $b' \ ^1\Sigma_u^+, v=1$ (lower part) vibronic states. The dots refer to the deviations between energy positions derived from both P and R lines and unperturbed levels (dashed line) as calculated from the spectroscopic constants of table 3 (with $H_{c_4, b'} = 0$).

Because of low signal-to-noise ratio, quoted uncertainties for the c_3 -X lines are nominally 0.08 cm^{-1} , i.e. larger than the errors estimated for the c_4' -X band.

The experimental data on the observed P, Q and R branch of the c_3 -X band were fitted to an energy relation for a diatomic molecule in a Π state:

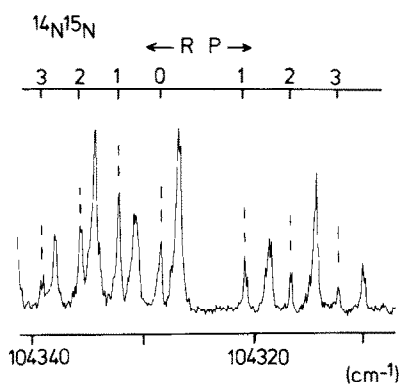


Fig. 4. XUV excitation spectrum of the $c_4^1\Sigma_u^+ - X^1\Sigma_g^+(0,0)$ band with TOF mass selector set at 29 mass units. The $^{14}\text{N}^{15}\text{N}$ resonances are assigned and marked by the vertical dashed lines.

$$E_{\Pi^+} = BJ(J+1) - DJ^2(J+1)^2 - q_\pi J(J+1) + q_\pi^D J^2(J+1)^2. \quad (2)$$

$$E_{\Pi^-} = BJ(J+1) - DJ^2(J+1)^2. \quad (3)$$

where q_π and q_π^D denote the A doubling and centrifugal correction parameter respectively. These equations are based on the assumption that only the Π^+ levels are shifted due to an interaction with a $^1\Sigma_u^+$ state, and that Π^- levels remain unperturbed. Within such a framework, where the specific Σ^+ perturber is not identified, the data of the c_3-X band were treated in a minimization routine. Good convergence (normalized $\chi^2 = 1.8$) was obtained when again excited states with $J \geq 20$ are omitted from the fit. The spectroscopic constants thus obtained are listed also in table 3. The differences between observed and calculated line positions, including the extrapolated values for $J \geq 20$, are given in table 5.

Table 4

Observed line positions (in cm^{-1}) for R(J) and P(J) lines of the $c_4^1\Sigma_u^+ - X^1\Sigma_g^+(0,0)$ band for the $^{14}\text{N}^{15}\text{N}$ molecule as well as deviations from a least squares fit. The uncertainty in the line positions is $0.06 \text{ cm}^{-1 \text{ a}}$

R(J)			P(J)	
J	observed	obs. - calc.	observed	obs. - calc.
0	104328.12	-0.05		
1	104331.81	0.06	104320.47	-0.14
2	104335.16	-0.02	104316.78	0.15
3	104338.44	-0.03	104312.54	0.03

^a) Spectroscopic constants for the $c_4^1(0)$ state of $^{14}\text{N}^{15}\text{N}$ are: $B = 1.855(3) \text{ cm}^{-1}$ and $\nu_1 = 104324.46(3) \text{ cm}^{-1}$. D was fixed at $6 \times 10^{-5} \text{ cm}^{-1}$.

In order to facilitate the interpretation of the nature of the A doubling in the $c_3^1\Pi_u, v=0$ state the observed splittings between $\Pi^+(J)$ and $\Pi^-(J)$ levels are plotted in fig. 6. The splittings are derived from energy differences between R($J-1$) and Q(J) lines, and P($J+1$) and Q(J) lines, respectively. Using eqs. (2) and (3) and the q_π and q_π^D parameters from table 3 the splittings can be reproduced accurately for values up to $J=20$. However, due to the large centrifugal correction term $q_\pi^D J^2(J+1)^2$ the model predicts a decrease of A -doublet splittings for $J > 20$, as shown by the dashed curve in fig. 6. The deviation between observed and extrapolated (for $J > 20$) transition frequencies in table 5 indicate that predominantly the Π^+ components with high J value do not follow the model. For $\Pi^-(J)$ states observed in the Q-branch deviations from eq. (3) are less, but nevertheless, significant.

Carroll and Yoshino [8] have reported that a description of the two lowest Rydberg states c_3 and c_4 in terms of a "p complex" within l -uncoupling theory is not possible because of the strong homogeneous perturbations of particularly the c_3 state. Nevertheless we attempted to calculate the A -doublet splittings in such a model. For each J a matrix of the form

$$\begin{pmatrix} E_{c_4} & H_{c_4c_3} & 0 \\ H_{c_4c_3} & E_{c_3\Pi^+} & 0 \\ 0 & 0 & E_{c_3\Pi^-} \end{pmatrix}$$

was diagonalized. In the theory of l -uncoupling the interaction matrix element between two Rydberg states of $^1\Pi$ and $^1\Sigma$ character within a p complex is given by [8,24,25]

$$H_{c_4c_3} = 2B_{av} \sqrt{J(J+1)}, \quad (4)$$

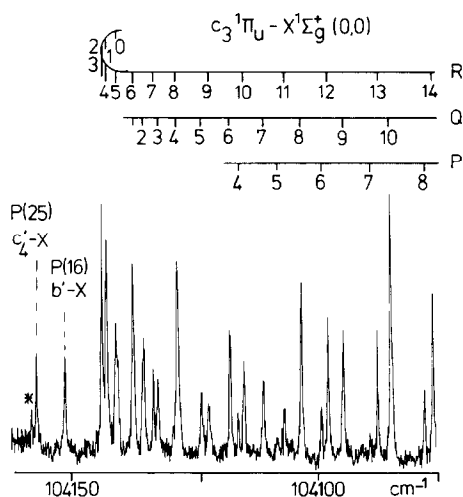


Fig. 5. Recorded XUV excitation spectrum of the bandhead part of the $c_3 \ ^1\Pi_u - X \ ^1\Sigma_g^+ (0, 0)$ band. (*) Unidentified.

with B_{av} the averaged rotational constant of the two interacting states. With the rotational constants of table 3 an average rotational constant for the c_3 - c'_4 complex of $B_{av} = 1.72 \text{ cm}^{-1}$ is obtained. For this value of B_{av} the doublet splittings between Π^+ and Π^- levels in $c_3 \ ^1\Pi_u, v=0$ were calculated. The results are plotted as the dotted curve in fig. 6.

In a treatment of the energy levels of the $c_3 \ ^1\Pi_u, v=0$ state the strong homogeneous mixing of this Rydberg state with the vibrational ladder of $b \ ^1\Pi_u, v$ states cannot be ignored. An important result of a de-perturbation analysis of Stahel et al. [10] is that the $c_3(0)$ state has a wavefunction composition of

$$|c_3(0)\rangle' = 0.58|c_3(0)\rangle + 0.55|b(4)\rangle \\ - 0.49|b(5)\rangle .$$

In this analysis only the two largest admixtures of other vibronic states were considered, thus neglecting contributions of other $b \ ^1\Pi_u, v$ states. A de-perturbed rotational constant of $B = 1.957 \text{ cm}^{-1}$ was found for the $c_3(0)$ Rydberg state. The $c'_4 \ ^1\Sigma_u^+, v=0$ state was found to be an almost pure Rydberg state with only minor admixture of $b' \ ^1\Sigma_u^+, v$ vibronic states of valence character:

$$|c'_4(0)\rangle' = -0.99|c'_4(0)\rangle + 0.06|b'(1)\rangle \\ + 0.04|b'(11)\rangle .$$

By considering only the pure Rydberg character of the c_3 - c'_4 complex, so setting $B_{av} = 1.94 \text{ cm}^{-1}$ and introducing a 0.58 weighing factor for the off-diagonal matrix element the A -doublet splittings were calculated again. The results are given as the full curve in fig. 6.

4. Discussion

In the preceding section the high-resolution data on the $c_3 \ ^1\Pi_u$ and $c'_4 \ ^1\Sigma_u^+$ Rydberg states were analyzed as independent band systems, with a single perturbation by a valence band in the case of c'_4 . Such a treatment appeared to be quite successful although deviations occurred for $J > 20$ states in both $c_3 \ ^1\Pi_u$ and $c'_4 \ ^1\Sigma_u^+$. Stahel et al. [10] have explained the extremely irregular sequence of band origins of $b \ ^1\Pi_u, v$ states in terms of strong homogeneous Rydberg valence interactions with the lowest $c_3 \ ^1\Pi_u, v=0$ state. Similar homogeneous interactions between states of $^1\Sigma_u^+$ symmetry were also investigated and found to be less pronounced. Regarding the complexity of the problem and the large energy shifts caused by the mutual perturbations (on the order of several hundred cm^{-1}) the model of Stahel et al. describes the positions of the vibronic origins well. However, deviations between calculations and observations are still on the order of several cm^{-1} . For a perturbation analysis describing the highest resolution data on rotational states a model with an accuracy of 0.04 cm^{-1} is required. It will also be necessary to include data on rotational states of all perturbing vibronic sequences in the energy range between 100000 and 105000 cm^{-1} to obtain a complete description. Particularly information on high J rotational states of several homogeneously interacting vibrational states is lacking. Therefore we chose to give a preliminary account of our high resolution data in terms of a simplified local model with an a posteriori semi-quantitative discussion of additional perturbing effects. A more comprehensive treatment awaits the analysis of the vast amount of high-resolution synchrotron data, which is presently under way [26].

In order to tentatively identify the origin of the perturbing effects a plot of all $^1\Pi$ and $^1\Sigma^+$ states in N_2 in the energy range under investigation is presented in fig. 7. Apart from our data also absorption

Table 5

Observed line positions (in cm^{-1}) for R(J), Q(J) and P(J) lines of the $c_3 \ ^1\Pi_u-X \ ^1\Sigma_g^+$ (0, 0) band. The position of unblended lines was determined to within 0.08 cm^{-1}

R(J)			Q(J)		P(J)	
J	observed	obs. – calc.	observed	obs. – calc.	observed	obs. – calc.
0	104141.60 ± 0.08	0.14				
1	104143.40 ± 0.08	–0.03	104137.75 ± 0.20	0.22		
2	104144.37 ± 0.08	0.00	104135.76 ± 0.08	0.15	104129.62 ± 0.08	0.09
3	104144.37 ± 0.08	0.06	104132.78 ± 0.08	0.06		
4	104143.40 ± 0.08	0.16	104128.87 ± 0.08	0.02	104116.43 ± 0.08	–0.09
5	104141.60 ± 0.20	0.45	104124.04 ± 0.08	0.01	104108.51 ± 0.08	0.00
6	104137.75 ± 0.20	–0.30	104118.15 ± 0.08	–0.07	104099.41 ± 0.08	–0.06
7	104133.74 ± 0.08	–0.19	104111.36 ± 0.08	–0.07	104089.60 ± 0.08	0.17
8	104128.82 ± 0.08	0.02	104103.56 ± 0.08	–0.09	104078.28 ± 0.08	–0.11
9	104122.42 ± 0.08	–0.21	104094.91 ± 0.08	0.03	104066.23 ± 0.08	–0.08
10	104115.30 ± 0.08	–0.15	104085.03 ± 0.08	–0.07	104053.13 ± 0.08	–0.10
11	104107.06 ± 0.08	–0.19	104074.20 ± 0.08	–0.11		
12	104098.02 ± 0.08	0.01	104062.52 ± 0.08	0.03	104023.91 ± 0.08	–0.09
13	104087.93 ± 0.08	0.20	104049.67 ± 0.08	0.02	104007.92 ± 0.08	0.07
14	104076.54 ± 0.08	0.12	104035.77 ± 0.08	0.02	103990.66 ± 0.08	–0.02
15	104064.15 ± 0.08	0.07	104020.83 ± 0.08	0.05	103972.47 ± 0.08	–0.00
16	104050.81 ± 0.08	0.13	104004.82 ± 0.08	0.07	103953.25 ± 0.08	0.01
17	104035.77 ± 0.20	–0.46	103987.59 ± 0.08	–0.03	103933.01 ± 0.08	0.04
18	104020.79 ± 0.08	0.07	103969.48 ± 0.08	0.10	103911.84 ± 0.08	0.19
19	104003.97 ± 0.08	–0.17	103950.03 ± 0.08	0.01	103889.56 ± 0.08	0.28
20	103986.09 ± 0.08 ^{a)}	–0.42	103929.42 ± 0.08	–0.09	103865.92 ± 0.08	0.06
21	103966.91 ± 0.08 ^{a)}	–0.88	103907.81 ± 0.08 ^{a)}	–0.03	103841.12 ± 0.08	–0.27
22	103946.63 ± 0.08 ^{a)}	–1.37	103884.78 ± 0.08 ^{a)}	–0.21	103815.40 ± 0.08 ^{a)}	–0.45
23	103924.92 ± 0.08 ^{a)}	–2.20	103860.39 ± 0.08 ^{a)}	–0.48		
24	103902.04 ± 0.08 ^{a)}	–3.11	103834.86 ± 0.08 ^{a)}	–0.79		
25	103877.56 ± 0.08 ^{a)}	–4.52	103808.02 ± 0.08 ^{a)}	–0.99		
26	103852.05 ± 0.08 ^{a)}	–5.84	103779.72 ± 0.08 ^{a)}	–1.59		
27			103750.07 ± 0.08 ^{a)}	–2.13		
28			103718.88 ± 0.08 ^{a)}	–2.89		
29			103686.53 ± 0.08 ^{a)}	–3.45		

^{a)} Not used in the minimization routine.

data of Carroll and Collins [7] on the $b \ ^1\Pi_u$, $\nu=4, 5$ and 6 valence states and emission data of Wilkinson and Houk [3] on the $b' \ ^1\Sigma_u^+$, $\nu=0, 1$ and 2 valence states are included. $^1\Sigma_u^-$ states, that might play a role as perturbers, have not yet been found in this region. An overview graph as fig. 7 gives insight in the occurrence of local perturbations. In addition to the anti-crossing $c'_4(0)$ – $b'(1)$ near $J=10$ another perturbation shows at $J=22$ between $b(4)$ and $b'(0)$ states. Wilkinson and Houk indeed found energy shifts of 2.35 cm^{-1} in the P(23) and R(21) lines of emission bands from $b'(0)$.

At the highest J states observed the $c'_4(0)$ levels approach $b(5)$ levels. The $c'_4 J=25$ level is shifted

downwards by 6.8 cm^{-1} from the value derived from the rotational constants of table 4. The $c'_4(0)$ state was also studied in emission to the $X \ ^1\Sigma_g^+$, $\nu''=1$ state by Tilford and Wilkinson [4]. These emission data were reanalyzed with the present accurate spectroscopic constants for the excited $c'_4(0)$ state and the constants for $X \ ^1\Sigma_g^+$, $\nu''=1$ [1]. We found that the J numbering of the c'_4 – $X(0, 1)$ data is correct and that energies of $c'_4(0)$ $J>20$ levels again deviate from calculated values. In table 6 the observed emission data of the c'_4 – $X(0, 1)$ P branch are listed with deviations from calculations. In the original analysis [4] deviations on the order of 40 cm^{-1} were reported, but in a re-analysis the transition frequencies of Tilford and

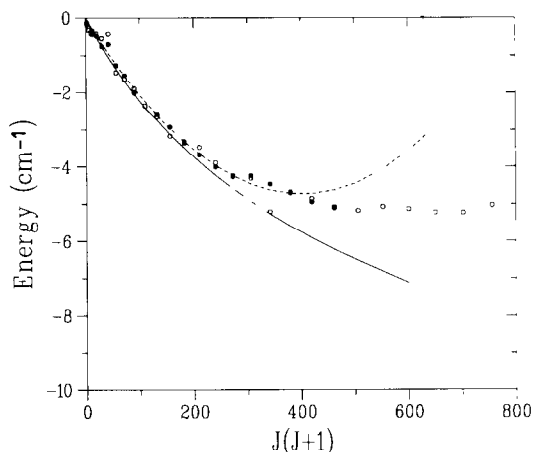


Fig. 6. Experimental A -doublet splittings (in cm^{-1}) between Π^+ and Π^- levels of the $c_3 \ ^1\Pi_u, v=0$ state as a function of $J(J+1)$. The negative value shows that Π^+ levels are shifted downward in energy. Open circles (respectively black dots) are obtained from differences between R (respectively P) and Q-branch lines. The dashed line represents the values calculated from the constants of table 3. The dotted curve is based on calculations within l -uncoupling theory with $B_{2v}=1.72 \text{ cm}^{-1}$ (see text); the full curve is based on calculations of l -uncoupling with only the Rydberg character of the c_3 - c_4 complex taken into account.

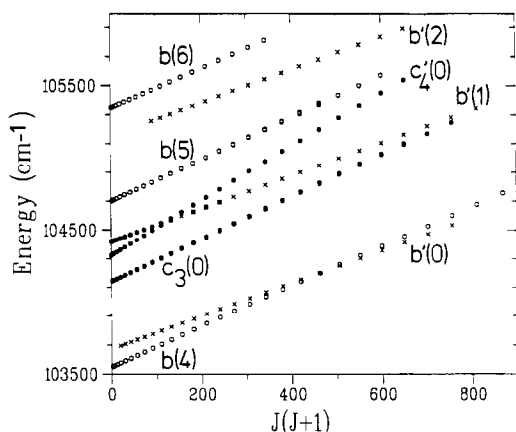


Fig. 7. Term values (in cm^{-1}) for all known rovibronic singlet states of N_2 in the denoted energy range as a function of $J(J+1)$. The points are derived from listed transition frequencies and subsequent addition of the ground state energies. (\circ) ref. [7]; (\times) ref. [3]; (\bullet) present investigation.

Wilkinson for the c_4 -X (0,1) band were found to be consistent with those of the c_4 -X (0,0) band observed in emission by Yoshino and Tanaka [12]. The

Table 6

Line positions in the P branch of the $c_4 \ ^1\Sigma_u^+ - X \ ^1\Sigma_g^+ (0, 1)$ emission band as observed by Tilford and Wilkinson [4] and deviations from calculated values from spectroscopic constants of table 3

	P(J) line observed	obs. - calc.
21	101880.0	-0.0
22	101871.0	-0.6
23	101861.6	-1.0
24	101851.0	-2.2
25	101839.0	-4.1
26	101826.5	-5.9
27	101810.4	-10.7
28	101793.4	-15.6

differences between term values derived in a straightforward manner from the emission data and the values extrapolated from rotational constants are found to be up to 15 cm^{-1} for $J=27$. The energy shifts of high J $c_4(0)$ states of tables 1 and 6 agree well in view of the experimental uncertainties.

It can be concluded that for $J > 20$ levels large energy shifts occur in the $c_4(0)$ state. It is also known that the A doubling in the $b \ ^1\Pi_u, v=5$ states is exceptionally large [7], that it grows rapidly at high J values and that the Π^+ states are shifted upwards in energy with respect to Π^- states. Such a A doubling can only be caused by a $^1\Sigma_u^+$ state lower in energy than the $b(5)$ state. These facts indicate that most probably a heterogeneous interaction between $c_4(0)$ and $b(5)$ causes the A doubling in $b \ ^1\Pi_u, v=5$ as well as the downward shifts of high J states of the $c_4 \ ^1\Sigma_u^+, v=0$ state. From the trend in the deviations between observed and extrapolated values for the transition frequencies in the c_4 -X (0, 1) emission band, as listed in table 6, it follows that a crossing between interacting $c_4 \ ^1\Sigma_u^+, v=0, J$ and $b \ ^1\Pi_u, v=5, J$ (only Π^+) levels cannot occur for $J \leq 27$. Around this interaction point a perturbation with a frequency jump of more than 30 cm^{-1} is to be expected in the P and R branches of bands involving $c_4(0)$ and $b(5)$ states.

Under the assumption that the downward shift on the $c_4(0)$ state is caused by a heterogeneous interaction with $b(5)$ an estimate can be given for the interaction parameter. The off-diagonal matrix element is represented by [11,25]

$$\langle c'_4(0), J | H | b(5), J \rangle = H_{c_4 b_5} \sqrt{J(J+1)}. \quad (5)$$

At $J=25$ the splitting between energy levels of $c'_4(0)$ and $b(5)$ is 140 cm^{-1} . This follows from an extrapolation of the data of Carrol and Collins on $b(5)$ [7], and the present data on $c'_4(0)$. The shift at $J=25$ in $c'_4(0)$ caused by the perturbation is 6.85 cm^{-1} . This yields a value for the interaction parameter of $H_{c_4 b_5} = 1.24 \text{ cm}^{-1}$.

Extrapolated term values predict a crossing of $c'_4 \ ^1\Sigma_u^+$, $v=0$ and $b' \ ^1\Sigma_u^+$, $v=2$ states in between $J=33$ and 34 . Here the spectroscopic constants for the $b'(2)$ state were taken from ref. [3]. From calculated overlap integrals [10] an interaction parameter of $H_{c_4 b_2} = 12.0 \text{ cm}^{-1}$ is expected. A homogeneous perturbation of this strength will induce shifts in the $c'_4(0)$ levels of -6.0 cm^{-1} at $J=34$ and a shift of -0.5 cm^{-1} at $J=27$. Although the direction is right, the magnitude of these predicted shifts of $c'_4(0)$ is much smaller than those observed in XUV excitation as well as emission. Therefore we conclude that the interaction with the $b'(2)$ state does not explain the deviations at high J states.

Eqs. (2) and (3) for the description of the A doubling in the $c_3(0)$ state give a mathematically correct representation of the energy levels, at least for $J < 20$. However, a physical explanation of the $\Pi^+ - \Pi^-$ splittings in terms of a specific perturber is not obtained. For all Rydberg complexes $c_n \ ^1\Pi_u$ and $c'_{n+1} \ ^1\Sigma_u^+$ (for $n > 3$) the theory of " l uncoupling" was shown to explain the A -doublet splittings in the $^1\Pi_u$ Rydberg states well [8].

Because of the strong homogeneous mixing of the $c_3 \ ^1\Pi_u$ state with valence states belonging to the $b \ ^1\Pi_u$ v vibronic manifold [10] a straightforward application of " l -uncoupling" theory (without accounting for this mixing) to the c_3 - c'_4 complex does not reproduce the observed A -doublet splittings in the $c_3(0)$ state (see dotted line in fig. 6). In that case the predicted values for the splittings between Π^+ and Π^- levels in $c_3(0)$ are too large by a factor of three. However, if only the Rydberg fraction in the wavefunctions of the c_3 and c'_4 states and deperturbed values for the rotational constants are taken [10], then the calculated A -doublet splittings obtained from l uncoupling agree with the observed values, at least up to $J=15$ (see full curve of fig. 6). It should be noted here that the framework of l uncoupling used, is a

model without any adjustable parameters. For rotational states $J > 15$ the predicted values are again larger than the observed splittings. This might be an indication for a rotational dependence for the Rydberg valence mixing between $c_3 \ ^1\Pi_u$ and $b \ ^1\Pi_u$, v states. From the analysis of the homogeneous perturbation between the $c'_4 \ ^1\Sigma_u^+$, $v=0$ and $b' \ ^1\Sigma_u^+$, $v=1$ states we obtain a mixing coefficient of 0.05, representing the $b'(1)$ valence fraction of the $c'_4(0)$ state. This only holds away from the interaction point at $J=10, 11$. At $J=11$ we find a larger admixture of $b'(1)$ valence character and a pure Rydberg character of $(0.88)^2$ for the $c'_4(0)$ state. This has however no consequence for the l -uncoupling model and the A -doublet splittings in the $c_3(0)$ state, because the $b'(1)$ state for $J=11$, at the same term energy, makes up for the complementary amount of Rydberg character.

A crossing of energy levels of $c_3(0)$ and $b'(1)$ is predicted in between $J=28$ and 29 based on energies calculated from the spectroscopic constants (see also fig. 7). The question arises whether the A doubling in the $c_3 \ ^1\Pi_u$ state may be partly caused by an additional heterogeneous interaction with the nearby valence state $b' \ ^1\Sigma_u^+$, $v=1$. This matter cannot be settled by the interpretation of only the presently obtained data, because levels $b' \ ^1\Sigma_u^+$, $v=1$ with $J > 15$ were not excited. However, inspection of the rather accurate emission data of Wilkinson and Houk [3] yields information on rotational states up to $J=31$. These data on the $b' \ ^1\Sigma_u^+ - X \ ^1\Sigma_g^+$ (1, 7), (1, 8), (1, 9) and (1, 11) bands were analyzed in a minimization routine using as fixed parameters the spectroscopic constants for the excited states from table 3. Also the interaction with the $c'_4 \ ^1\Sigma_u^+$, $v=0$ state was included. For each band the fit converged remarkably well: normalized $\chi^2 = 1.0$ with errors set at 0.15 cm^{-1} . Some of the lines reported by Wilkinson and Houk were found to deviate more than 0.5 cm^{-1} from calculated values: R(17) in the (1, 7) band, R(14) and P(17) in the (1, 8) band, R(10) in the (1, 9) band and P(15) in the (1, 11) band. As these deviations do not reproduce in the different emission bands they are considered to be accidental calibration errors. Surprisingly even for high J values (up to $J=31$) no systematic deviations occurred, although the upper state energies were calculated from rotational constants determined in the $J=1-15$ range. At the same time this

Table 7

Resulting spectroscopic parameters for the X $^1\Sigma_g^+$, v'' states of N_2 (all in cm^{-1}) from a fit of Wilkinson and Houk [3]. In the minimization routine on the $b' ^1\Sigma_u^+ - X ^1\Sigma_g^+$ ($1, v''$) bands the constants for the excited state were fixed at the values given in table 3. The centrifugal distortion constants $D_{v''}$ were fixed at the values predicted from the rotational and vibrational parameters (see ref. [3])

v''	$B_{v''}$	$D_{v''}$	$\nu_{0v''}$
7	1.8684 ± 0.0001	0.568×10^{-5}	15706.3 ± 0.5
8	1.8517 ± 0.0002	0.567×10^{-5}	17834.0 ± 0.5
9	1.8331 ± 0.0001	0.566×10^{-5}	19933.7 ± 0.5
11	1.7971 ± 0.0001	0.564×10^{-5}	24045.2 ± 0.5

implies that a possible heterogeneous interaction between $b' ^1\Sigma_u^+$, $v=1$ and $c_3 ^1\Pi_u$, $v=0$ does not give rise to significant shifts (larger than 0.2 cm^{-1}) and may therefore be neglected. Thus we conclude that the A doubling in the $c_3 ^1\Pi_u$ state is not affected by the $b' ^1\Sigma_u^+$, $v=1$ state.

Of course on theoretical grounds mixing between the $c_3(0)$ and $b'(1)$ is not expected, because the molecular orbital (MO) configurations for both states differ by two orbitals [5,28].

As a byproduct of the re-analysis of emission data we obtained accurate spectroscopic constants for the X $^1\Sigma_g^+$, $v=7, 8, 9$ and 11 states of N_2 . The results are listed in table 7. The errors in the rotational constants follow from the internal consistency of the fitting procedure while the uncertainty in the rotationless term values ν_i ($i=7, 8, 9$ and 11) is dependent on the absolute calibration of the Wilkinson and Houk experiment (0.5 cm^{-1}). Based on the analysis of their data on the $b'-X$ ($1, 11$) emission band Wilkinson and Houk concluded that the local perturbation near $b'(1)$, $J=10-11$ is of a heterogeneous nature. They report the observation of an asymmetric frequency shift below and above the perturbation point. In the present analysis both states involved in this local perturbation are analyzed and a symmetric pattern was found (see fig. 6). Frequencies for $b'-X$ ($1, 11$) transitions were calculated using the accurate spectroscopic constants for the $b' ^1\Sigma_u^+$, $v=1$ state (table 3) and including the effect of the homogeneous perturbation by the $c_4 ^1\Sigma_u^+$, $v=0$ state. For the X $^1\Sigma_g^+$, $v''=11$ state the constants of table 7 were taken. A value of $24045.216 \text{ cm}^{-1}$ as obtained from the fit (calibration uncertainty of 0.5 cm^{-1} neglected) was taken for ν_{11} . Apart from the P(15) line the differences between observations and calculations are within or close to the experimental uncertainty of 0.15

cm^{-1} . As no systematic deviations occur we conclude that the model for the local perturbation $b'(1)-c_4(0)$ is not invalidated by the emission data.

For reasons that the XUV-power dependence of wavelength is not calibrated and the cross sections of the second step in the $1+1$ ionization process are not known no detailed analysis of the line intensities is possible. Nevertheless the intensity behaviour in the P branch of the $b'-X$ transition clearly shows the effect of intensity borrowing near the local perturbation. The P(9) line is weak, but the intensity grows towards P(12) and then drops again. It is remarkable however that this effect is not reproduced in the R branch, where the R(10) is strong and the R($J>11$) lines do not appear at all. In the c_4-X band the intensities of R(11) to R(17) odd J transitions do not follow the 2:1 ratio governed by the spin statistics. These phenomena remain to be explained after careful power calibration tests of the XUV spectrometer to be performed in the near future. It should be noted here that the observed spectral intensities in $1+1$ resonance enhanced two-photon ionization studies do not simply reflect one-photon line strengths. The natural lifetimes of the excited states play a crucial role, not only in the linewidths but also in the intensities of $1+1$ two-photon spectra [14].

Acknowledgement

The authors wish to thank W. Hogervorst for many stimulating discussions and his ongoing support for the XUV-laser project. We thank J. Bouma for his excellent technical support with the construction of the XUV-laser source and K. Eikema for his assistance during measurements and interpretation of data. We have appreciated the valuable suggestions

by K. Yoshino and H. Lefebvre-Brion. Financial support from the Foundation for Fundamental Research on Matter (FOM) and the Netherlands Organization for the Advancement of Research (NWO) is gratefully acknowledged.

References

- [1] A. Lofthus and P.H. Krupenie, *J. Phys. Chem. Ref. Data* 6 (1977) 113.
- [2] R.E. Worley, *Phys. Rev.* 64 (1943) 207.
- [3] P.G. Wilkinson and N.B. Houk, *J. Chem. Phys.* 24 (1956) 528.
- [4] S.G. Tilford and P.G. Wilkinson, *J. Mol. Spectry.* 12 (1964) 231.
- [5] H. Lefebvre-Brion, *Can. J. Phys.* 47 (1969) 541.
- [6] K. Dressler, *Can. J. Phys.* 47 (1969) 547.
- [7] P.K. Carroll and C.P. Collins, *Can. J. Phys.* 47 (1969) 563.
- [8] P.K. Carroll and K. Yoshino, *J. Phys. B* 5 (1972) 1614.
- [9] K. Yoshino, Y. Tanaka, P.K. Carroll and P. Mitchell, *J. Mol. Spectry.* 54 (1975) 87.
- [10] D. Stahel, M. Leoni and K. Dressler, *J. Chem. Phys.* 79 (1983) 2541.
- [11] K. Yoshino and D.E. Freeman, *Can. J. Phys.* 62 (1984) 1478.
- [12] K. Yoshino and Y. Tanaka, *J. Mol. Spectry* 66 (1977) 219.
- [13] T. Trickl, E.F. Cromwell, Y.T. Lee and A.H. Kung, *J. Chem. Phys.* 91 (1989) 6006.
- [14] W. Ubachs, L. Tashiro and R.N. Zare, *Chem. Phys.* 130 (1989) 1.
- [15] J.M. Ajello, G.K. James, B.O. Franklin and D.E. Shemansky, *Phys. Rev. A* 40 (1989) 3524.
- [16] D.F. Strobl and D.E. Shemansky, *J. Geophys. Res.* 87 (1982) 1361.
- [17] P.F. Levelt, W. Ubachs and W. Hogervorst, to be published.
- [18] A. Lago, Ph.D. Thesis, University of Bielefeld, Germany (1987).
- [19] S. Gerstenkorn and P. Luc, *Atlas du spectre d'absorption de la molecul de l'iode entre 14800–20000 cm^{-1}* (CNRS, Paris, 1978).
- [20] S. Gerstenkorn and P. Luc, *Rev. Phys. Appl.* 14 (1979) 791
- [21] C.P. Rinsland, R. Zander, A. Goldman, F.J. Murray, D.G. Murray, M.R. Gunson and C.B. Farmer, *J. Mol. Spectry.* 148 (1991) 2741.
- [22] H. Lefebvre-Brion and R.W. Field, *Perturbations in the spectra of diatomic molecules* (Academic Press, New York, 1986).
- [23] J. Bendtsen, *J. Raman Spectry.* 2 (1974) 133.
- [24] R.S. Mulliken, *J. Am. Chem. Soc.* 86 (1964) 3183.
- [25] I. Kovacs, *Rotational structure in the spectra of diatomic molecules* (Hilger, London, 1969).
- [26] K. Yoshino, private communication.
- [27] M. Leoni and K. Dressler, *Helv. Phys. Acta* 45 (1972) 959.
- [28] H. Lefebvre-Brion and C.M. Moser, *J. Chem. Phys.* 43 (1965) 1394.